On simulation of transient thermal convection of two-fluid layers in a horizontal circular enclosure

C. J. Ho* and Y. H. Lin†

*Department of Mechanical Engineering, National Cheng Kung University, Tainan, Taiwan, Republic of China

†Department of Mechanical Engineering, National Pintung Institute of Agriculture, Pintung, Taiwan, Republic of China

This article presents a numerical simulation of the transient thermal convection phenomenon in a horizontal circular enclosure containing two immiscible fluids. To cope with the rather complex computational domain encountered when the volume ratio of the two fluids in the enclosure is not unity, a simple radial coordinate transformation technique is used to map the respective domains occupied by the fluids into half-circular ones. Numerical simulation by a finite-difference method is performed for air–water layers as the two-fluid system in the enclosure. The simulated fluid flow structure and temperature distributions are presented by means of contour maps of streamlines and isotherms.

Keywords: two-fluid layers; enclosure flows; transient thermal convection

Introduction

The thermal convection phenomenon in enclosed space containing multiple fluids has recently received increasing attention because of its fundamental importance and practical relevance to fuel storage systems, combustion processes, thermal energy storage systems, crystal growth processes, freezing processes, and so on. Compared to the number of investigations of thermal convection in enclosures filled with single fluid, relatively few reports of work concerning thermal convection in enclosed multiple fluids can be found in the literature.[1–13] Of this small number, however, most deal with the steady-state aspects of the problem. Thus knowledge about transient multifluid thermal convection in enclosures is still limited. A proper understanding of transient phenomena is essential to the design and operation of various engineering applications of thermal–fluid systems, such as the transient adjustment process of a confined multifluid layer to a sudden change in the externally imposed thermal conditions at the enclosure wall.

The present work is part of a research program whose objective is to provide further basic understanding and heat transfer data for the thermal convection in enclosures containing multiple immiscible fluids. Of practical interest is numerical simulation of transient thermal convection fluid-flow development and heat transfer characteristics in a horizontal cylindrical enclosure filled with two immiscible fluids subject to circumferential heating or cooling. Furthermore, the physical configuration studied can be viewed as an extension of the numerical analysis conducted in Reference 2, which considered only the situation of a half-filled gas–liquid layer; here the formulation presented can be easily adapted to the two-fluid enclosure for various volume ratios of the two fluids. Moreover, a numerical study of laminar natural convection in a partially filled horizontal cylinder subjected to heating but with an adiabatic free surface has already been performed by means of a rather complicated coordinate transformation method.[14]

Address reprint requests to Professor Ho at the Department of Mechanical Engineering, National Cheng Kung University, Tainan, Taiwan, Republic of China.

Received 5 December 1989; accepted 4 June 1990

Problem statement and mathematical formulation

As illustrated in Figure 1, the two quiescent fluids enclosed in a horizontal circular enclosure of radius R are initially at a uniform temperature T_i. The transient thermal convection is initiated by suddenly raising or lowering the wall temperature of the enclosure to an isothermal constant temperature T_o. Mathematical formulation of the physical problem was based on a cylindrical coordinate system that originated at the center of the fluid–fluid interface and on the following assumptions.

(1) The fluid flow is two-dimensional (2-D), laminar, and symmetrical about a vertical midplane of the enclosure.
(2) The fluids are Newtonian.
(3) The interface between the fluids is flat and the influence of the curved meniscus at the fluid–solid interface is neglected.

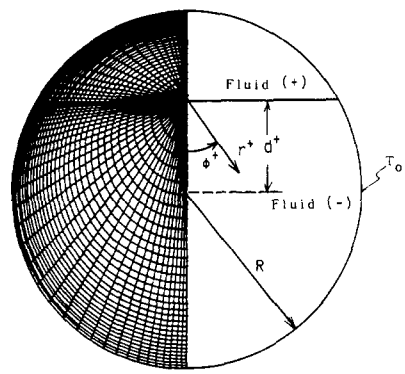

Figure 1 Physical configuration and grid system

(4) Effects of vaporization–condensation and mass transfer at the interface are neglected.
(5) The Boussinesq approximation is valid.
(6) Viscous dissipation and compressibility effects are negligible.

Furthermore, to cope with the rather complex computational domain encountered when the volume of the circular enclosure is not equally occupied by the two fluids, we utilized a simple radial coordinate transformation technique to map the domains occupied by the fluids into half-circular ones. We achieved this radial coordinate transformation by defining a new radial variable:

$$\eta=\frac{r}{F(\phi^+)} \tag{1}$$

where $F(\phi^+)$ denotes the radial profile of the circular enclosure measured from the center of the fluid–fluid interface and is of the form

$$F(\phi^+)=[1-d^2\ \sin^2(\phi^+)]^{1/2}-d\cos(\phi^+) \tag{2}$$

The positive/negative d designates the dimensionless distance of the fluid–fluid interface below/above the horizontal centerline of the circular enclosure, which in turn reflects the volume ratio of the two fluid layers in the enclosure.

In the transformed domain, the normalized governing equations for the problem can then be expressed in terms of vorticity, stream function, and temperature:

$$\frac{\partial\omega}{\partial\tau}+\frac{1}{\pi}\frac{\partial\eta}{\partial r}\left(\frac{\partial\psi}{\partial\phi}\frac{\partial\omega}{\partial\eta}-\frac{\partial\psi}{\partial\eta}\frac{\partial\omega}{\partial\phi}\right)=A\mathrm{Pr}_-\nabla^2\omega+B\mathrm{Ra}_-\times\left[\sin(\phi\pi)\frac{\partial\eta}{\partial r}\frac{\partial\theta}{\partial\eta}+\frac{\cos(\phi\pi)}{\pi r}\left(\frac{\partial\theta}{\partial\phi}+\frac{\partial\eta}{\partial\phi}\frac{\partial\theta}{\partial\eta}\right)\right] \tag{3}$$

$$\nabla^2\psi=-\omega \tag{4}$$

$$\frac{\partial\theta}{\partial\tau}+\frac{1}{\pi}\frac{\partial\eta}{\partial r}\left(\frac{\partial\psi}{\partial\phi}\frac{\partial\theta}{\partial\eta}-\frac{\partial\psi}{\partial\eta}\frac{\partial\theta}{\partial\phi}\right)=C\nabla^2\theta \tag{5}$$

where

$$\nabla^2\equiv\left[\left(\frac{\partial\eta}{\partial r}\right)^2+\left(\frac{1}{\pi r}\frac{\partial\eta}{\partial\phi}\right)^2\right]\left(\frac{\partial^2}{\partial\eta^2}\right)+\frac{2}{(\pi r)^2}\frac{\partial\eta}{\partial\phi}\frac{\partial^2}{\partial\eta\,\partial\phi}+\frac{1}{(\eta r)^2}\frac{\partial^2}{\partial\phi^2}+\left[\frac{1}{r}\frac{\partial\eta}{\partial r}+\frac{1}{(\eta r)^2}\frac{\partial^2\eta}{\partial\phi^2}\right]\frac{\partial}{\partial\eta} \tag{6a}$$

$$\frac{\partial\eta}{\partial r}=\frac{1}{F} \tag{6b}$$

$$\frac{\partial\eta}{\partial\phi}=-\frac{\eta}{F}\frac{\partial F}{\partial\phi} \tag{6c}$$

$$\frac{\partial^2\eta}{\partial\phi^2}=\frac{-1}{F}\left(\eta\frac{\partial^2F}{\partial\phi^2}+2\frac{\partial\eta}{\partial\phi}\frac{\partial F}{\partial\phi}\right) \tag{6d}$$

and

$$A=1,\quad B=1,\quad C=1 \qquad \text{for the lower fluid layer} \tag{6e}$$

$$A=\frac{1}{\nu_s},\quad B=\frac{1}{\beta_s},\quad C=\frac{1}{\alpha_s} \qquad \text{for the upper fluid layer} \tag{6f}$$

Initial conditions are

$$\text{at } \tau=0,\quad \psi=\omega=\theta=0 \tag{7}$$

Boundary conditions are

$$\phi=0 \text{ or } 1,\quad \psi=\omega=\frac{\partial\theta}{\partial\phi}=0 \qquad \text{(symmetric lines)} \tag{8a}$$

$$\eta=1,\quad \psi=\frac{\partial\psi}{\partial\eta}=0,\quad \theta=1 \tag{8b}$$

At the fluid–fluid interface, we assumed that the following conditions hold.

(1) Continuity of temperature and tangential velocity:

$$\theta_+=\theta_-;\quad u_+=u_- \tag{8c}$$

Notation

A	Heat transfer area
d	Vertical distance of interface to the center of the enclosure
F^+	Radial profile of the circular enclosure
F	Dimensionless radial profile of the circular enclosure, F^+/R
g	Gravitational acceleration
h	Heat transfer coefficient
k	Thermal conductivity
Ma_-	Marangoni number
Nu	Nusselt number
Pr_-	Prandtl number
r^+	Radial coordinate
r	Dimensionless radial coordinate, r^+/R
R	Radius of the circular enclosure
Ra_-	Rayleigh number
t	Time
T	Temperature
T_i	Initial temperature
T_o	Isothermal surface temperature of the enclosure
u	Radial velocity
v	Angular velocity

Greek symbols

α	Thermal diffusivity
β	Thermal expansion coefficient
η	Radial coordinate in transformed plane
θ	Dimensionless temperature, $(T-T_i)/(T_o-T_i)$
Λ	Nusselt number
ν	Kinematic viscosity
ρ	Density
σ	Surface tension
τ	Dimensionless time, $\alpha_- t/R^2$
ϕ^+	Angular coordinate
ϕ	Dimensionless angular coordinate ϕ^+/π
ψ^+	Stream function
ψ	Dimensionless stream function ψ^+/α_-
ω^+	Vorticity
ω	Dimensionless vorticity ω^+R^2/α_-

Subscripts

$+, -$	Upper and lower fluid, respectively
f	Interface between the fluids
s	Ratio of the lower fluid to the upper fluid

Superscript

$\bar{}$	Circumferentially averaged quantity

(2) Impermeability:

$$v_+ = v_- = 0 \tag{8d}$$

(3) Continuity of heat flux:

$$k_s\left(\frac{\partial\theta}{\partial\phi}+\frac{\partial\eta}{\partial\phi}\frac{\partial\theta}{\partial\eta}\right)_+ = \left(\frac{\partial\theta}{\partial\phi}+\frac{\partial\eta}{\partial\phi}\frac{\partial\theta}{\partial\eta}\right)_- \tag{8e}$$

(4) Continuity of shear stress:

$$\mu_s\left(\frac{\partial u}{\partial\phi}+\frac{\partial\eta}{\partial\phi}\frac{\partial u}{\partial\eta}\right)_+ = \left(\frac{\partial u}{\partial\phi}+\frac{\partial\eta}{\partial\phi}\frac{\partial u}{\partial\eta}\right)_- - \mathrm{Ma}_-\pi r\frac{\partial\eta}{\partial r}\frac{\partial\theta}{\partial\eta} \tag{8f}$$

where the Marangoni number Ma_- reflects the relative strength of surface tension and viscous shear.

Inspection of the foregoing formulation reveals the dimensionless parameters for the problem:

$$\mathrm{Ra}_- = \frac{g\beta_-(T_o - T_i)R^3}{\nu_-\alpha_-}$$

$$\mathrm{Ma}_- = \frac{(d\sigma/dT)(T_o - T_i)R}{\alpha_-\mu_-}$$

$$\mathrm{Pr}_- = \frac{\nu_-}{\alpha_-}$$

$$\nu_s = \nu_+/\nu_-, \quad \mu_s = \frac{\mu_+}{\mu_-}, \quad \alpha_s = \frac{\alpha_+}{\alpha_-},$$

$$k_s = \frac{k_+}{k_-}, \quad \beta_s = \frac{\beta_+}{\beta_-}, \quad d = \frac{d^+}{R}$$

For a specified pair of immiscible fluids, the number of dimensionless parameters is considerably less. In that case, Ra_-, Ma_-, and d are the relevant parameters.

Numerical method

We made the solution domain of the problem discrete by means of a nonuniform grid mesh, as shown in Figure 1. The grid mesh has a smoothly varying grid spacing, denser near the solid boundary and at the fluid–fluid interface to account for the steep gradient of the field variables in these regions. We used three different grid systems resulting from a series of grid-size tests for the computations, depending on the position of the fluid–fluid interface as listed in Table 1.

We then solved the governing differential equations, equations 3–5, subject to the boundary conditions, equations 7–9, by a finite-difference method, using forward difference for the time derivatives and central difference for the spatial derivatives, except the convective terms for which we applied the second upwind approach.[15] We solved the discrete form of equations 3 and 5 numerically by an implicit procedure and the stream function equation, equation 4, by the modified strongly implicit procedure.[16] For each time step we continued an iterative solution procedure until a relative convergence criterion of 10^{-5} was satisfied for each field variable. We used a time step as small as 10^{-4} for the transient calculations at high Rayleigh number.

Table 1 Grid systems

	Region	
d	−	+
0.5	35 × 21	35 × 33
0.0	35 × 25	35 × 25
−0.5	35 × 33	35 × 21

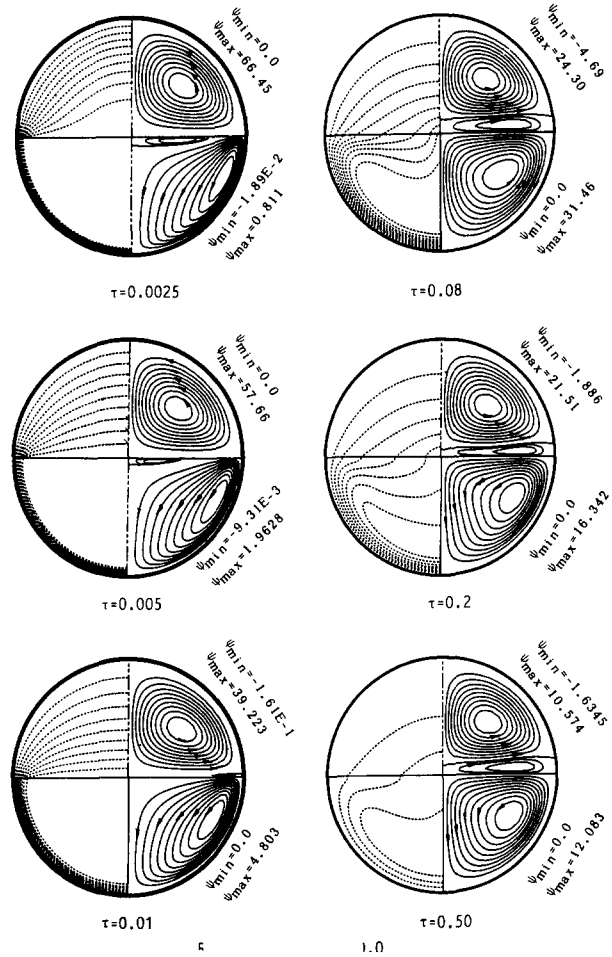

Figure 2 Transient flow development and temperature field for $\mathrm{Ra}_- = 10^5$, $\mathrm{Ma}_- = 0$, and $d = 0$

Results and discussion

We performed numerical simulation for the air–water layers of the two-fluid system in the enclosure ($\nu_s = 15.86$, $\mu_s = 0.0198$, $\alpha_s = 152.2$, $k_s = 0.043$, and $\beta_s = 18.50$). The ranges of the relevant parameters covered were: $d = -0.5$, 0.0, and 0.5; $\mathrm{Ra}_- = 10^3$ to 10^7; and $\mathrm{Ma}_- = 0$ to 10^4. Here, we considered only the heating process.

Development of flow and temperature fields

The simulated fluid flow structures and temperature distributions are presented as contour maps of streamlines (solid lines) and isotherms (dashed lines), respectively. Figures 2 and 3 present the transient development of thermal convection phenomenon during the heating process for $\mathrm{Ra}_- = 10^5$ and 10^7, respectively, with $d = 0$ and $\mathrm{Ma}_- = 0$. In general and as anticipated, convective motion in the air-filled region developed rather rapidly, and a counterclockwise flow structure had already formed at the early time. For $\mathrm{Ra}_- = 10^5$ (Figure 2), convective flow in the water region starts with weak circulation along the water-wetted wall of the enclosure and a secondary eddy below the air–water interface. The isotherms show that the temperature in the water region is more or less unaffected at the early time, because it has a thin thermal boundary layer confined near the wall. As time passes, more of the water is

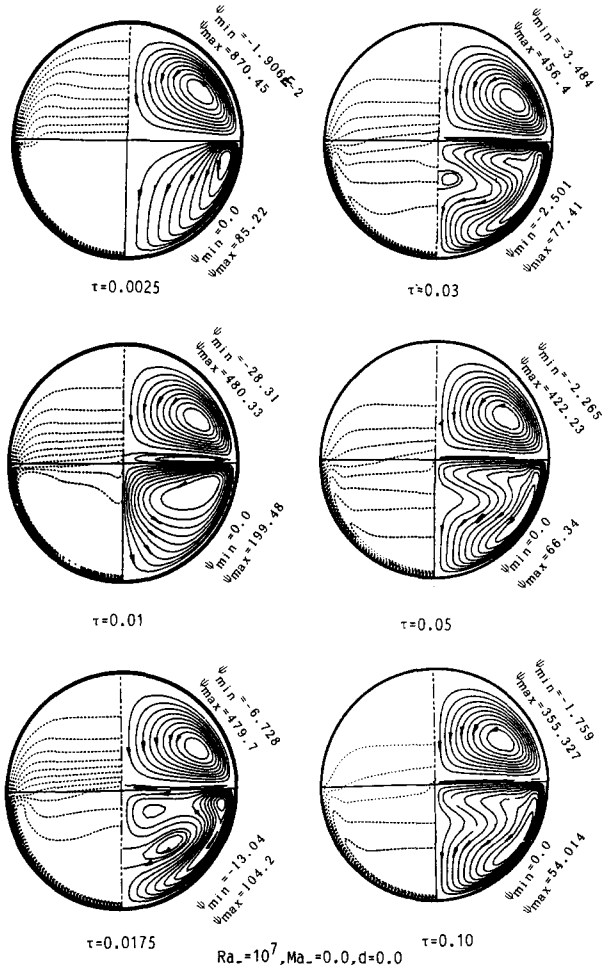

Figure 3 Transient flow development and temperature field for $Ra_- = 10^7$, $Ma_- = 0$, and $d = 0$

heated by the solid wall—as well as by the heat transported across the air–water interface—and the temperature gradients in both regions tend to decrease. The main circulation of water tends to intensify and move toward the vertical symmetrical line of the enclosure, suppressing the secondary eddy beneath the interface. As a result, at $\tau = 0.01$, the secondary eddy in the water region is seen to disappear. However, the flow of air tends to weaken gradually with the decaying temperature gradient, and a secondary eddy develops above the air–water interface near the solid wall. At $\tau = 0.08$, the flow structure in the enclosure is characterized by a clockwise air eddy between the counterclockwise circulations of the air and water. As the heating process continues and the temperature gradient in the water becomes smaller, the convection motion of the water also begins to decay.

With increasing Rayleigh number, the transient flow structure and temperature distribution evolve somewhat differently from those for $Ra_- = 10^5$. For $Ra_- = 10^7$ (Figure 3), flow development in the water layer features an innermost eddy in the horizontal isothermal core as the isotherm fronts tend to penetrate downward from the air–water interface. This development may be rationalized as a result of path adjustment of the downward-penetrating hot (light) stream along the central symmetry line of the enclosure as it encounters the cold (heavy) isothermal core of the water. Similarly, the innermost eddy had been predicted by the numerical simulation of transient natural convection inside a partially glycerine-filled horizontal circular vessel with an adiabatic free surface.[14]

The influence of the position of the air–water interface, namely, the volume ratio of the two fluids, on the flow structures and isotherm patterns is shown in Figure 4 for $Ra_- = 10^6$, $Ma_- = 0$, and $d = 0.5$ and -0.5. With the enclosure containing more water, the convective flow of water and the secondary air eddy above the interface are markedly enhanced; an opposite effect occurs for the main circulation of air.

Figures 5 and 6 illustrate the effect of surface tension at the air–water interface. Figure 5 presents a situation for purely thermocapillary-driven convection, which may occur under extraterrestic condition ($g = 0$). In the absence of a buoyancy force, fluid flow in both the air and water regions appears to develop simultaneously from the interfacial region in the vicinity of the solid wall. The counterrotating flow structure exhibiting some symmetry with respect to the interface can be readily observed for the enclosure filled half with air and half with water. However, in the presence of a buoyancy force, surface tension tends to aid development of buoyant flow in water while hindering it in air. Accordingly, as shown in Figure 6 for $Ra_- = 10^3$ and $Ma_- = 10^3$, the buoyant flow structure developed early in the air is gradually displaced by the growing thermocapillary-driven circulation. Eventually at the later time, $\tau = 0.05$, the buoyant flow of air is replaced completely by the clockwise thermocapillary circulation. The higher value of ψ_{max} in the water region in Figure 6 (compared with Figure 5) clearly reflects the augmented flow strength resulting from the coupling of thermocapillary and buoyancy forces.

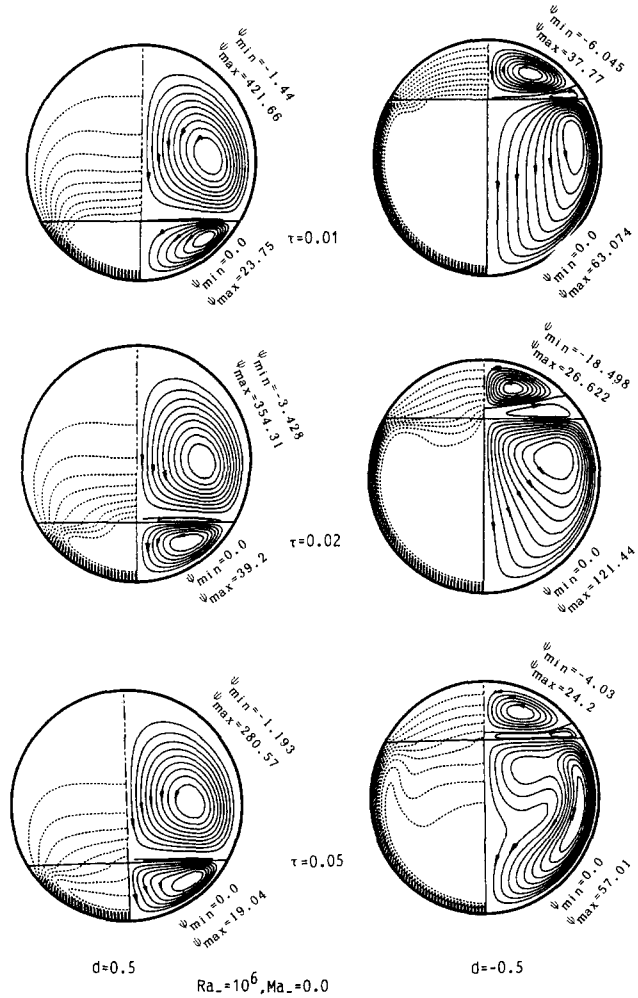

Figure 4 Transient flow development and temperature field for $d = 0.5$ and -0.5, with $Ra_- = 10^6$ and $Ma_- = 0$

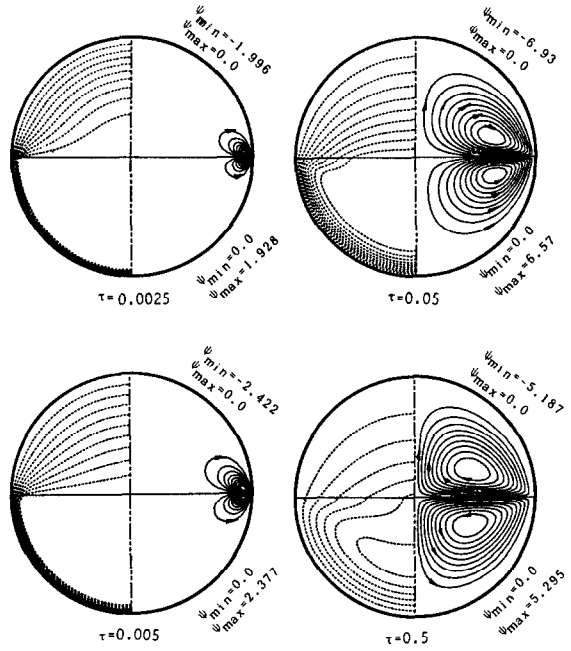

Figure 5 Development of thermocapillary convection for $Ma_- = 10^3$, $Ra_- = 0$, and $d = 0$

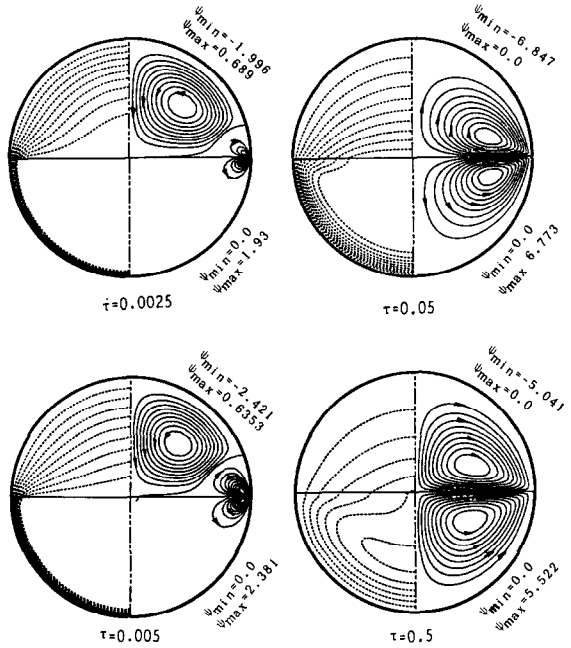

Figure 6 Development of combined buoyancy and thermocapillary convection for $Ma_- = 10^3$, $Ra_- = 10^3$, and $d = 0$

Heat transfer results

We now turn to the results of transient heat transfer during the heating process. Figure 7 typifies the angular variation of the local heat transfer rate during the heating process for $Ra_- = 10^5$, $d = 0$, and $Ma_- = 0$ by means of a local Nusselt number defined as

$$Nu_o = D\left[1+\left(\frac{1}{\pi F}\frac{\partial F}{\partial \phi}\right)^2\right]^{1/2}\frac{\partial \eta}{\partial r}\frac{\partial \theta}{\partial \eta}\bigg|_{\eta=1} \tag{9}$$

where

$$D = \begin{cases} k_s & \text{for the upper fluid-wetted portion} \\ 1 & \text{for the lower fluid-wetted portion} \end{cases}$$

During the early period, $\tau \leq 0.01$, a uniform heat flux distribution prevails over the water-wetted wall, while a significant angularly decreasing trend already exists for the air-wetted portion of the enclosure surface. This condition further reflects the previously mentioned rapid development of buoyant convection in the air-filled region. Furthermore, a sudden drop-off of the Nusselt number across the air–water interface as indicated in Figure 7 is apparently due to the lower thermal conductivity of the air above the interface. Most important, the local Nusselt number continues to decrease, as expected, as the heating process proceeds. Figures 8–10 show the temporal history of the average Nusselt number for the purely buoyancy-induced convection along the air- or water-wetted enclosure surface—or the entire surface of the enclosure—which are defined, respectively, as

$$\overline{Nu}_+ = \frac{1}{A_+}\int_{A_+} Nu_o \, dA_+ \tag{10a}$$

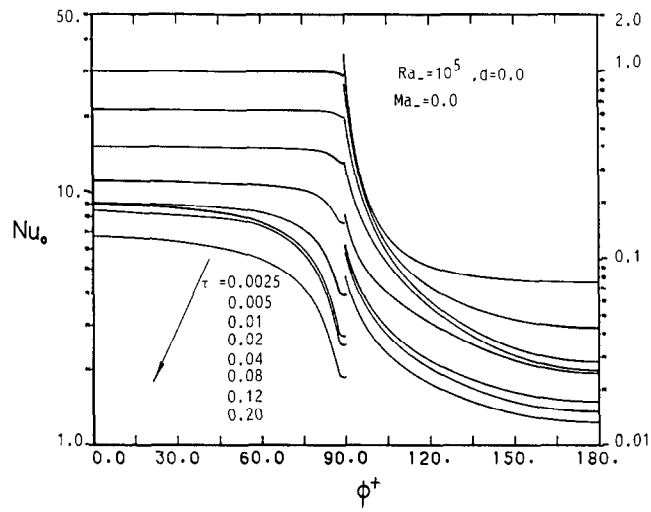

Figure 7 Angular variation of local Nusselt number on enclosure surface

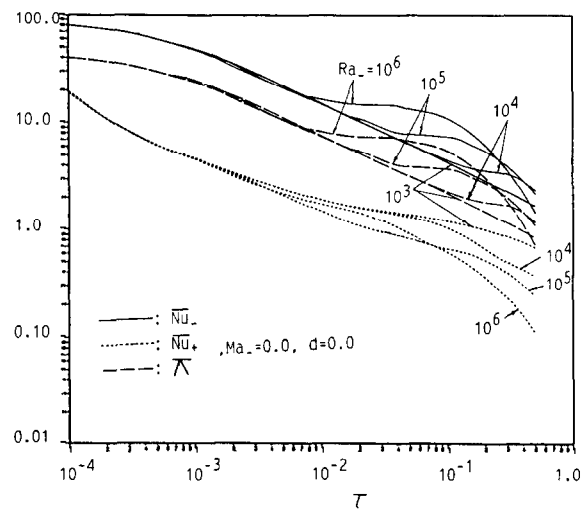

Figure 8 Temporal variation of the average Nusselt number for $d = 0$ and $Ma_- = 0$

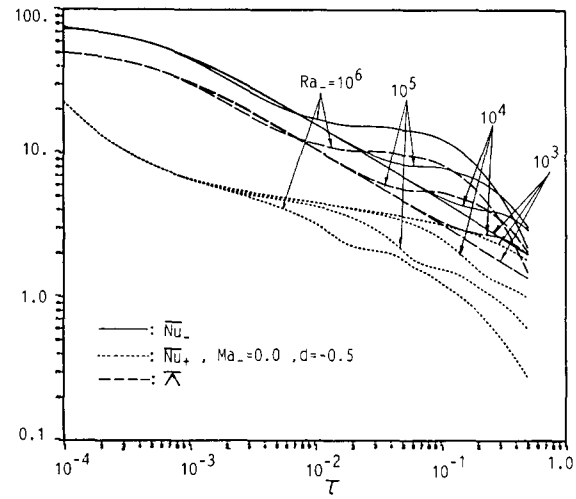

Figure 9 Temporal variation of the average Nusselt number for $d=-0.5$ and $Ma_-=0$

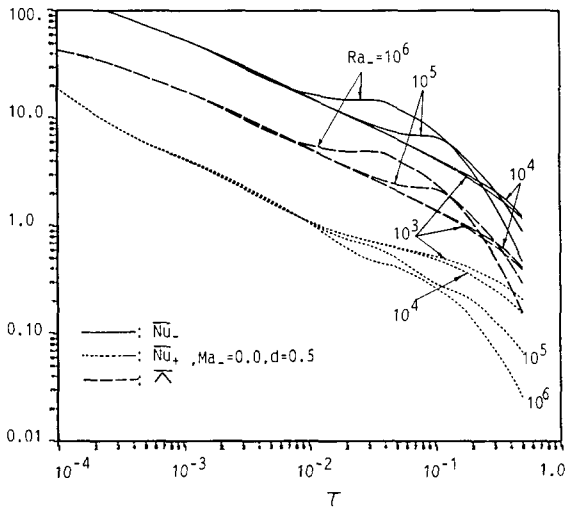

Figure 10 Temporal variation of the average Nusselt number for $d=0.5$ and $Ma_-=0$

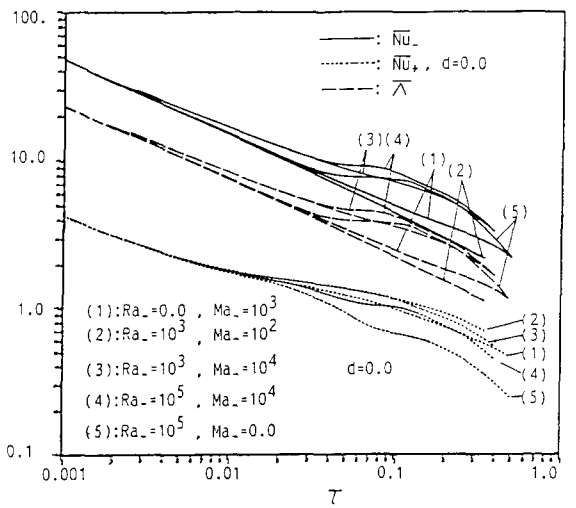

Figure 11 Effect of surface tension on the average Nusselt number for $d=0$

$$\overline{Nu}_- = \frac{1}{A_-}\int_{A_-} Nu_o \, dA_- \tag{10b}$$

$$\overline{\Lambda} = \frac{A_+\overline{Nu}_+ + A_-\overline{Nu}_-}{A_+ + A_-} \tag{10c}$$

Figures 8–10 reveal that, as expected, prior to full development of buoyancy-induced flow, heat transfer is dominated by the conduction mechanism, as evidenced by the clustered curves for various Rayleigh numbers at the early stage of the heating process. Moreover, the average Nusselt number for the air-wetted surface is an order of magnitude lower than that on the water-wetted surface. Consequently, the timewise variation of the average Nusselt number for the entire wall of the enclosure displays a qualitative trend similar to that for the water-wetted portion. This result clearly suggests that the water layer is the dominant heat transfer fluid in the air–water-filled enclosure. Closer examination of Figures 8–10 indicates further that among the three different values of d considered, the case of the enclosure half filled with air and half filled with water, $d=0$, provides a better overall heat transfer environment for the process of heat-up.

Finally, the influence of the surface tension on the average heat transfer rate is illustrated in Figure 11. It shows that the interfacial surface tension tends to aid the overall convective heat transfer rate, particularly at the low Rayleigh number.

Concluding remarks

A numerical simulation was formulated for transient thermal convection in a horizontal circular enclosure containing two immiscible fluids. A simple radial coordinate transformation technique was utilized to cope with the rather complex computational domain encountered when the volume of the enclosure is not occupied equally by the two fluids. Numerical simulation by a finite-difference method was performed for air–water layers comprising the two-fluid system in the enclosure. The purpose was to provide some insight into the transient thermal convection flow development and heat transfer characteristics during heating of the two-fluid layer. Results of the simulations demonstrate that buoyant convection in the air-filled region of the enclosure develops more rapidly than that in the water-filled region. The transient flow fields and temperature distributions in the air–water-filled enclosure can be significantly affected by the presence of thermocapillary-driven convection at the interface. Moreover, the water layer is the dominant heat transfer fluid in the enclosure; interfacial surface tension tends to enhance the transient overall convective heat transfer rate, particularly at the low Rayleigh number.

Corresponding experimental work is needed to verify the numerical simulations obtained. Also, additional simulations based on the present formulation should be conducted to investigate the transient thermal convection phenomena in the horizontal circular enclosure containing other immiscible fluid pairs of engineering interest.

Acknowledgment

This work was supported by a grant from the National Science Council of Republic of China, NSC76-0401-E006-13. Also the helpful comments made by reviewers are greatly appreciated.

References

1 Knight, R. W. and Palmer, M. E. Simulation of free convection in multiple fluid layers in an enclosure by finite difference. In

Numerical Properties and Methodologies in Heat Transfer, T. M. Shih, ed. Hemisphere, Washington D.C., 1983, 305–319

2 Oosthuizen, P. H. and Kuhn, D. Unsteady free convection flow in a circular container half-filled with liquid and half-filled with gas. In *Heat Transfer in Enclosure*, R. W. Douglass and A. F. Emery, eds. ASME HTD—Vol. 39, 1984, 1–11

3 Projan, U. and Beer, H. Theoretical and experimental study of transient and steady-state natural convection heat transfer from a vertical flat plate partially immersed in water. *Int. J. Heat Mass Transfer*, 1985, **28**, 1487–1498

4 Sparrow, E. M., Azevedo, L. F. A., and Prata, A. T. Two-fluid and single-fluid natural convection heat transfer in an enclosure. *ASME J. Heat Transfer*, 1986, **108**, 848–852

5 Myrum, T. A., Sparrow, E. M., and Prata, A. T. Numerical solutions for natural convection in a complex enclosed space containing either air–liquid or liquid–liquid layers. *Num. Heat Transfer*, 1986, **10**, 19–43

6 Aggarwal, S. K., Iyengar, J., and Sirignano, W. A. Enclosed gas and liquid with non-uniform heating from above. *Int. J. Heat Mass Transfer*, 1986, **29**, 1593–1604

7 Sparrow, E. M. and Myrum, T. A. Experiments on natural convection in complex enclosed space containing either two fluids or a single fluid. *Int. J. Heat Mass Transfer*, 1987, **30**, 1247–1258

8 Projan, U. and Beer, H. Thermogravitational and thermocapillary convection heat transfer in concentric and eccentric horizontal cylindrical annuli filled with two immiscible fluids. *Int. J. Heat Mass Transfer*, 1987, **31**, 93–107

9 Abranzon, B., Edwards, D. K., and Sirignano, W. A. Transient stratified enclosed gas and liquid behavior with concentrated heating from above. *AIAA J. Thermophys. and Heat Transfer*, 1987, **1**, 355–364

10 Villers, D. and Platten, J. K. Thermal convection in superimposed immiscible liquid layers. *Appl. Sci. Res.*, 1988, **45**, 145–152

11 Kimura, T., Heya, N., Takeuchi, M., and Isomi, H. Natural convection of fluids with stratified two fluid layers in rectangular enclosure. *Trans. JSME, B*, 1985, **51**, 1251–1259

12 Kimura, T., Heya, N., Takeuchi, M., and Isomi, H. Natural convection heat transfer in rectangular enclosure contained fluids with stratified two layers. *Trans. JSME, B*, 1986, **52**, 617–626

13 Ho, C. J. and Lin, Y. H. Thermal convection heat transfer of air/water layers enclosed in horizontal annuli with mixed boundary conditions. *Wärme-und Stoffübertragung*, 1989, **24**, 211–224

14 Aydemir, N. U., Sousa, A. C. M., and Venart, J. E. S. Transient laminar free convection in horizontal cylinder. *Wärme-und Stoffübertragung*, 1986, **20**, 59–67

15 Roache, P. J. *Computational Fluid Dynamics*, Hermosa, Albuquerque, NM, 1976

16 Schneider, G. E. and Zedan, M. A modified strongly implicit procedure for the numerical solution of field problems. *Num. Heat Transfer*, 1981, **4**, 1–19